The tectonized central peak of the Mjølnir impact crater (Barents Sea)

Romain Corseri[1,*], Sébastien Gac[2], Jan Inge Faleide[2,3,4], Sverre Planke[1,3,4]

Manuscript accepted for publication at Journal of Structural Geology

[1]Volcanic Basin Petroleum Research AS, Oslo Science Park, Gaustadalléen 21, N-0349 Oslo, Norway

[2]Department of Geosciences, University of Oslo, Boks 1047 Blindern 0316 Oslo, Norway

[3]Centre for Earth Evolution and Dynamics, University of Oslo, Box 1028 Blindern, 0315 Oslo, Norway

[4]Research Centre for Arctic Petroleum Exploration, University of Tromsø, Tromsø, Norway

[*]Corresponding author: romain.corseri@gmail.com / romain@vbpr.no - Mob: +47 97487906

Abstract

The Mjølnir structure (Barents Sea) is one of the best-preserved marine impact craters on Earth. After impact on the paleo-seafloor, ~142 Ma ago, this crater experienced an atypical upward deformation of its central peak, now elevated ~435 m above the rims. We investigate the effect of far-field tectonic stresses on central peak vertical motions based on interpretation of high-resolution P-Cable and conventional reflection seismic data. The reconstruction of the crater sedimentary infill history supports a subdued original central peak relief: a 5 km-wide, gentle mound lying ~15 m below the rim level. We found that subvertical, outward-dipping, impact-induced faults were reactivated, elevating segments of the central peak up to ~500 m above the platform during at least one post-Albian event. Previously seen as the main deformation mechanism, differential compaction may have tenuously increased the original central peak height by ~10 m after burial by marine shales. The mobilization of Triassic impact-shattered rock by tectonic compression beneath the central peak provide a robust explanation for the structural rise. We postulate that a Cenozoic tectonic compression event triggered uplift of Mjølnir central peak and doming of nearby salt structures in the SW Barents Sea.

Keywords

Impact crater; Mjølnir; Central peak; Post-impact modification; Tectonic reactivation; Compression

1. Introduction

The study of impact craters is fundamental to understand the geological and biological evolution of our planetary system. In 2012, the Gale Crater was selected as landing site for the Mars exploration rover Curiosity and illustrates the importance of impact studies for space exploration programs and our future society (Golombek et al., 2012). On Earth, 190 impact craters have been formally identified (Earth Impact Database on 30th of September, 2019), but it is known that 100s to 1000s are missing from the registry mainly due to post-impact modification such as burial, erosion and plate tectonics (Grieve et al., 1992).

Impact crater are divided into two groups: the simple craters are relatively small, bowl-shaped depression whereas complex craters are wider with a smaller depth-to-diameter ratio and a central peak, or peak ring, resulting from the uplift of impact-damaged rocks. At the crater edge, the rims consist of bedrocks elevated above the ground level and are usually the highest topographic point of impact structures (Poelchau et al., 2009).

Mjølnir is one of the few confirmed marine complex impact crater on Earth (Poag et al., 2004). Since the Early Cretaceous impact on the paleo-Barents Sea (Fig. 1), ~142 Ma ago, the original crater floor was almost entirely preserved from surficial processes due to the rapid crater burial and relatively stable sedimentary platform (Tsikalas et al., 1998c). The particularity of Mjølnir lies in its prominent central peak, presently rising ~435 meters above the crater rims and surrounding sedimentary platform, thus defying usual morphometric trends of impact craters (Tsikalas et al., 1998a). This atypical deformation of Mjølnir's central peak is a proven post-impact feature (Tsikalas et al., 1998b; Tsikalas and Faleide, 2007) and is unique, so far, in the registry of terrestrial impacts. This peculiar crater deformation has been attributed to differential compaction, resulting from ~2 km of post-impact sediment loading around the central high (Tsikalas and Faleide, 2007; 2010). This hypothesis is largely based on the presence of a

positive Bouguer and seismic travel time anomaly at the central peak (Tsikalas et al., 1998c), arguably originating from the presence of a denser core of brecciated and uplifted Jurassic – Triassic rocks. However, density measurements of cores of the central peak at borehole 7329/03-U-01 (Fig. 1) display lower values than unaltered rocks of the sedimentary platform (Werner and Torsvik, 2010). This is in contradiction with the main argument for differential compaction offsetting the central peak ~435 m above the original impacted level. In this study, we explore an alternative causative mechanism for the uplift of Mjølnir's central peak. The several salt domes in the vicinity of Mjølnir (Fig. 1) are testimony of past compressional tectonic regimes in the SW Barents Sea. Could the fate of the Mjølnir structure also be linked to far-field tectonic stresses?

We test this hypothesis for the first time with modern geophysical datasets acquired for petroleum exploration in the past decade. In this work, we revisit the 40 km-wide Mjølnir impact crater (Gudlaugsson, 1993) in the Barents Sea (Fig. 1) based on interpretation of recent 2D high-resolution P-Cable and conventional seismic reflection data. These modern 2D seismic datasets provide a unique window to cratering processes and post-impact modification at Mjølnir. We unveil a solid set of evidences supporting a main mechanism for post-impact crater modification by tectonic stresses and reactivation of deep syn-impact faults at Mjølnir's central peak.

We aim at fulfilling three objectives: (1) A detailed characterization of the crater sedimentary infill (2) A reconstruction of the vertical motions of the central peak from original crater floor to present-day (3) A revision of the structural configuration of the Mjølnir impact structure.

2. Structural configuration of the Mjølnir crater

About 142 Ma ago, an extra-terrestrial bolide impacted the bottom of the paleo-Barents Sea forming a complex impact crater on the sedimentary platform (Fig. 1). The crater was quickly

buried by marine sediments and subsequently preserved from surficial processes (Fig. 2). Discovered in the early 90's by Steinar T. Gudlaugsson, Mjølnir is established unequivocally as a latest Jurassic (Tithonian) – earliest Cretaceous (Berriasian) marine complex impact crater (Dypvik and Attrep, 1999; Gudlaugsson, 1993). It was scrutinized in numerous multidisciplinary scientific publications, ranging from geophysical data and corehole interpretation, impact and tsunami numerical modelling to environmental consequences (e.g. Dypvik et al., 2004, 2010; Shuvalov et al., 2002; Glimsdal et al., 2007; Tsikalas et al., 1998a, b, c).

Mjølnir is a 40 km-wide complex crater, with well-defined rim faults generated minutes after impact, during the gravitational collapse stage of the cratering process (Collins et al., 2012). The various crater domains (i.e. outer domain, annular basin and central peak) and the "inverted-sombrero" shape of the disturbance zone have been formally identified in vintage seismic data (Tsikalas et al., 1998b). The three main stages of the impact-cratering processes are (Collins et al., 2012): (1) contact and compression, (2) excavation/compression and ejecta emplacement and (3) modification.

However, the Mjølnir complex crater stands-out from other documented terrestrial craters with its highly deformed central peak, rising to ~435 meters above the crater rims and surrounding Bjarmeland Platform (Figs. 1 and 3a). Despite the Quaternary glacio-erosive processes (Sættem et al., 1992; Bellwald et al., 2018), the prominent central peak has been almost entirely preserved from erosion. Here, Mjølnir's central peak vertical motions will be at the center of attention.

The central peak of impact craters, also referred to as "central uplift" or "central high", is formed during the modification stage of the cratering process by the uplift of deep-impacted target rocks (Collins et al., 2012). Its formation is complex and the mechanics behind the rebound of deep-impacted rocks are still poorly understood (Kenkman et al., 2014). Some

terrestrial examples suggest a brittle behavior with both concentric and radial, subvertical faults in the vicinity of the central peak (Kenkmann et al., 2014). Central peaks are usually subtle post-impact topographic highs, rarely reaching the rims and impacted surface level. Therefore, Mjølnir's prominent central peak rising ~435 meters above the crater rims (Fig. 3a) is an oddity in the inventory of terrestrial craters. This unusual deformation was first attributed to differential compaction due to sediment loading (Tsikalas and Faleide, 2007, 2010). This explanation was largely based on a positive residual gravity and seismic travel time anomalies from at the central peak location. These anomalies could be reproduced by a density model that includes an abnormally dense core of uplifted rocks beneath the central peak. According to Tsikalas et al. (1998c), the surrounding crater domains and the sedimentary platform have subsided ~435 meters beneath the denser central high, under the load of post-impact sediments. However, the differential compaction hypothesis was considerably challenged by in-situ density measurements of 24 core samples of the central peak at borehole 7329/03-U-01 (Fig. 1) showing density values that are lower than the un-impacted strata of the Bjarmeland Platform (Werner and Torsvik, 2010). The effect of tectonism on late post-impact modification at Mjølnir central peak was not investigated in previous contributions, perhaps due to limited seismic data coverage, well calibration and a yet immature knowledge of the regional tectonic events.

3. Data and method

3.1 Seismic data

The P-Cable technology (Planke and Berndt, 2004) is a high-resolution seismic acquisition system, designed to allow a very high near-offset trace density and a uniform trace distribution. The system provides unparalleled high-resolution imaging of the subsurface and can achieve meter-scale resolution in the shallow subsurface. It has been used with success to map shallow reservoirs and glacial landforms in the Barents Sea (Bellwald et al., 2019; Corseri et al., 2018;

Lebedeva-Ivanova et al., 2018). P-Cable wide-azimuth seismic with 16 streamers and 6.25 m inline separation have been acquired in the Mjølnir area in 2015 (Fig. 1). The seismic stratigraphy in the vicinity of the central peak is scrutinized in two P-Cable sections, line 1 and line 2 crossing the center of the crater (Figs. 3, 4 and 5). In addition, we use conventional 2D reflection seismic data acquired between 2006 and 2014 by TGS and Fugro (Fig. 6). These regional seismic lines are used to tie deeper reflectors to the stratigraphy of the nearby Norvarg Dome of the Bjarmeland Platform (Fig. 1) and identify faults in the impact-disrupted area.

3.2 Stratigraphic concept

We retain the seismic stratigraphic nomenclature first defined by Tsikalas at al. (1998b) using markers from borehole 7430/10-U-01 (Fig. 1). There, LB "Lower Boundary", TD "Top Disturbance" and UB "Upper Boundary" (Figs. 2 and 3) reflectors constrain the stratigraphic position of the impact event. Reflector TD marks the level of unambiguous ejecta signature and shocked quartz grains (Tsikalas et al., 1998a). The post-impact interval is bounded by the TD and URU surfaces (Fig. 2) and will be investigated considering recent sedimentological studies on the depositional dynamics of the Early Cretaceous Barents Sea (Fig. 2; Grundvåg et al., 2017; Corseri et al., 2018; Midtkandal et al., 2019a). The Ragnarok Fm. is composed of allochthonous breccia (Unit I in Fig. 2) and debris flows, tsunami deposits due to violent reworking of sediments during the drowning of the central peak (Unit II in Fig. 2; Dypvik et al., 2004). In the high-resolution P-Cable seismic sections, a total of 10 horizons were picked in the early post-impact (LB to TD in Fig. 2) to late post-impact intervals (NW1, NW2, NE4, NE3a, NE3b to URU in Fig. 2).

In the late post-impact interval, five horizons reflects the recent advances in the knowledge of the Early Cretaceous stratigraphy of the Bjarmeland Platform (Fig. 1). NW1, NW2, NE4, NE3a, NE3 are seismic reflectors belonging to mud-rich prograding units infilling the epicontinental sea from early Barremian to Albian (Fig. 2; Midtkandal et al., 2019a). The LB horizon, i.e.

Lower Boundary , represents the base of the allochthonous breccia units (Fig. 2). Near the crater central, LB is likely marking a sharp transition between uplifted Jurassic and Triassic megaslabs forming the central peak to early post-impact allochthonous breccia (resp. unit I and unit II in Fig. 2; Dypvik et al., 2004).

An important aspect of the high-resolution seismic interpretation work on Mjølnir is to ensure the correct continuity of the horizons across each sides of the central peak. The top of the central peak was sheared by Plio-Pleistocene glacial erosion so most post-impact horizons were truncated by URU (Figs. 3 and 4). To ensure correct continuity of all post-impact reflectors across the sheared central peak, we used the seismic horizon flattening tool and verified that the internal seismic character and discernible reflections of each facies was continuous across each flank, starting from UB (Fig. 3b) and sequentially up to NE3b (Fig. 5b). Using this methodology, all post-impact horizons were correlated across the erosional truncation.

In the pre-impact stratigraphy, four Triassic horizons (Intra Snadd, Top Kobbe, Top Klappmyss, Top Havert) are picked in 2D conventional seismic data. The Top Permian horizon, TP, is the deepest distorted horizons in the platform stratigraphy (Fig. 6; Tsikalas et al., 1998b). Regardless of the seismic data type, all horizons, except NW1, were picked on negative amplitudes. The Triassic and Permian marker horizons were tied to available well tops of well 7225/3-1 on the Norvarg Dome and propagated to the crater area (Fig. 1).

The seismic interpretation was done in the time domain using the software Kingdom Suite v. 2014. Depth conversion is done by dividing the observed two-way time thickness by 2 and then multiplying the one-way time with the average internal velocity of 2900 m/s. This velocity is a representative average for the Lower Cretaceous post-impact succession [TD-URU] at Mjølnir based on interval velocities from well 7324/2-1 located on the western Bjarmeland Platform (Fig. 1; Faleide et al., 2019). Correcting for compaction effects is only relevant when we address original thicknesses, topography at time of deposition when we reconstruct the

crater relief by flattening. In such case, a likely scenario is a ~2 km, dominantly fine-grained overburden at Mjølnir (Ktenas et al., 2017), and a 15% decompaction factor is applied to all thickness measurements (Midtkandal et al., 2019b).

4. Post-impact stratigraphy

4.1 Seismic interpretation

4.1.1 Seismic facies

The results of the high-resolution seismic interpretation (Figs. 3a and 4) will be described from oldest [LB-TD] to youngest [NE3b-URU] seismic facies (Fig. 2).

[LB-TD] is underlain by the LB pick, a rugged, discontinuous, negative-amplitude reflector only discernible in the annular basin and central peak domains. LB is developing as faulted "steps", up to the central peak domain from the annular basin. The LB horizon has no radial symmetry across the central peak. Some structural expression such as horst-like structures are observed at the central peak summit and the northern flank of the central peak along line 2 (Fig. 4), within the eastern annular basin along line 1 (Fig. 3a). The [LB-TD] interval displays a transparent seismic character and has a maximal thickness of 10 ms (~15 m) in the annular basin and gradually thins-out toward the crater center, where it is absent. A faint internal reflection onlaps the horst-like structure along line 2. At present, the maximum variation of elevation of LB is ~350 ms (~510 m), from the summit of the central peak to the lowermost discernible reflection in the annular trough. In the outer crater domain (Fig. 3), the interval displays a transparent to chaotic seismic character. Its thickness smoothly increases from ~3 ms (~4 m) to ~8 ms (~10 m) at the rim of the crater. The interval is densely faulted and we observe collapse graben structures in its easternmost part of line 1 (Fig. 3). TD is a prominent negative-amplitude marker, easily picked along seismic lines. It is important to keep in mind that TD corresponds to the original crater floor (Tsikalas et al., 1998c).

[TD-UB] marks the return to “normal” marine sedimentation and drapes the original crater relief. The unit is composed of organic-rich, marine shales of the upper part of the Hekkingen Formation (Dypvik et al., 2004). It has a distinct seismic signature with 3 to 4 full seismic cycles with relatively continuous, conformable, high-amplitude reflections. It is thickest, 55 ms (~80 m), in the annular basin and thins-out to 30 ms (~45 m) against the rim fault. On top of the central peak, 35 ms (~50 m) thick segments of [TD-UB] are uplifted up to the summit level and truncated by URU (Figs. 3a and 4). UB is the most continuous and brightest reflection encompassing both crater and platform area. As a result, UB is used as a flattened level when reconstructing the original crater morphology (Fig. 3b). The open-marine shale interval is segmented by faults in the outer domain and highly deformed around the central peak flanks (see Section 4.1.2).

[UB-NW1] has also a transparent seismic character with a distinct wedge geometry towards the central peak flanks. There, NW1 onlaps onto the underlying UB horizon (Figs. 3a and 5; zoom 1 in Fig. 4). The NW1 horizon is gently dipping, downlapping onto UB, towards west along line 1 and south along line 2. Within the crater rims, the stratum is thickest, about 30 ms (~45 m), in the annular basin.

[NW1-NW2] shows internal clinoform surfaces and thins out from west to east along line 1 (Fig. 3a). It is thickest at the western rim, about 70 ms (~100 m). Along line 2, the unit has a distinct mound geometry as NW2 horizon downlaps onto NW1 on each side of the central peak (Fig. 4).

[NW2-NE4], [NE4-NE3a] and [NE3a-NE3b] share common characteristics in the P-Cable data. They gently dip in the westward direction (Fig. 3a) and mostly display an alternation of high-amplitude, continuous reflections and transparent layers. These internal patterns can be confidently identified across the URU truncation and are used to validate the reconstruction of the NE4, NE3a and NE3b horizon geometry across the URU truncation (Fig. 5).

4.1.2 Deformation

At the crater periphery, large faults are cross-cutting the whole post-impact sequence up to URU. These faults correspond to the rim faults and graben structures induced by gravitational collapse (Collins et al., 2012), east of line 1 (Fig. 3a). In this outermost area of the crater, the cumulative fault throw is around 20 ms (~30 m) in the post-impact interval. Note that within the grabens, the post-impact layers are also gently folded, seemingly deformed downward of up to 30 ms (~45 m).

Moving towards the center of the crater in the outer domain, we observe a higher fault density, but mostly restricted to the [LB-UB] interval. Faults have a short throw of 5 ms (~7 m). This faulting pattern is particularly evident on the eastern part of line 1 (Fig. 3a).

In the annular basin and in the vicinity of the central peak, a couple of faults are observed in the youngest post-impact interval within [NW2-URU]. Along line 2, we observe an atypical bedding imbrication pattern where the overburden starts flexuring (zoom 2 in Fig. 4).

At the central peak, outward dipping, high-angle faults offset the syn-impact LB horizon in several elevated “terraces”, segmenting the central peak. The fault throw is gradually increasing along the rising flanks of the central peak, up to 150 ms (~220 m) on the southern flank of line 2 (Fig. 4). Associated with these sub-vertical faults and terraces of the central peak, we note that the overlying Hekkingen Formation is subsequently deformed and fractured. A zoom on one of the “drag zone” shows that [TD-UB] is considerably thinned along the flanks of the central peak and fragmented by extensional faults (zoom 1 in Fig. 4, Fig. 5a). Importantly, these faults do not propagate to the overlying [NW1-NE3b] interval but generate gentle folds.

4.2 Original crater relief (TD)

The organic-rich marine shales of the Hekkingen formation were deposited as hemipelagic rain in an open-marine environment (Dypvik et al., 2004) and levelled the submerged crater, ~8 m.y.

after impact. Hence, the crater relief shortly after the impact can be restored when flattening the high-resolution lines along the UB horizon (Fig. 3b). We use an adequate decompaction factor of 15% (see Section 3.2). The original crater relief is represented by the TD horizon (Fig. 3b). The 40 km-wide original crater is a subtle topographic depression on the seabed, centered on a gentle central mound. Key morphometric points on Fig. 3b indicate that, shortly after impact, (1) the rims were the most elevated crater topography, rising ~1 ms (~2 m) above the platform level, (2) The annular basin represents the lowermost point of the crater depression, down to 30 ms (~50 m) below the rims and (3) The central peak is a smooth, 5 km-wide mound, rising 22 ms (~35 m) above the annular basin. Importantly, the summit of the central peak is still located 8 ms (~15 m) below the un-impacted platform level. This subtle crater relief with a quasi-absence of elevated rims is typical of marine impacts (Poag et al., 2004) and is remarkably consistent with shallow marine impact modelling predictions at Mjølnir using multimaterial hydrocode (Fig. 12 in Shuvalov et al., 2002). The original crater relief reconstruction from Tsikalas and Faleide (2007) indicates that the central peak was originally rising 80 m above the rim level. The reconstruction based on P-Cable seismic data significantly reduces the height of the original central peak after return of gravitational equilibrium, placing the central peak ~90 meters lower than Tsikalas and Faleide (2007). The reasons for this difference are that the seismic data used in Tsikalas and Faleide (2007) do not show uplifted segments of the Hekkingen formation above the central peak and that the semi-brittle thinning of the Hekkingen shales along its flanks can be misinterpreted as a depositional feature. The present reconstructions (Figs. 3b and 5b) are based on geometrical flattening where fault restoration is not applied. However, the quasi-absence of faults in post-impact interval of the annular basin and central peak domain, focus of this contribution, justify the use of simple flattening. In the outer domain, we observe that the short-lived faults affecting [TD-UB] (see Section 4.1.2) is barely distorting the original crater relief TD (Fig. 3b).

Comparing the original and present crater surface TD (Fig. 3), it is remarkable that the post-impact deformation mainly occurred in the inner annular through and within the central peak domain. In contrast, the elevation markers at the rim and outer annular trough show minor deformation in the outer crater domain after 142 m.y.

4.3 Crater infill history

In the previous section, we described the original central peak morphology (Fig. 3b) and entire crater morphology after draping by open-marine shales in Hauterivian. In Fig. 5b, we use flattening along the stratigraphic marker NE3b (Fig. 2) to restore the central peak morphology and post-impact stratigraphy in Albian, ~ 40 m.y. after impact. Above the truncation, we have reconstructed the missing horizons sequentially from NW2 to NE3b, assuming they were quasi-parallel to the crater drape UB (Fig. 5b). Although the uncertainty of the inferred picks increases with the length of the truncation, the remarkable conservation of the wedge geometries and internal reflectivity character of the low-angle prograding units across the central peak truncation validates the approach and give a high confidence in the reconstruction.

A striking observation when comparing the restored relief of the TD horizon in Albian (Fig. 5b) and Hauterivian (Fig. 3b) is that the central peak remained mostly inactive during this time span.

However, we note that NW1 onlaps UB on each side of the central peak (Figs. 3, 4 and 5) and provide the evidence of a minor vertical motion of the central peak as the UB horizon became a minor topographic high on the paleo-seabed while NW1 prograded in the crater in Barremian. We quantify this minor vertical displacement to 5 ms (~10 m). This minor central peak vertical motion is coeval with a short-lived tectonic event that segmented [TD-UB] in the outer crater domain (Fig. 3a). According to the post-impact reconstruction (Fig. 5b), this minor uplift of the central peak was quickly levelled by another prograding unit (NW2).

From Aptian to Albian, mud-rich units with low-angle clinoform surfaces (NE4, NE3) prograded NE-SW onto the central Bjarmeland Platform. The crater area was buried by up to ~670 meters of fine-grained marine sediments (Fig. 5b).

The present expression of the central peak shows a differential elevation of 350 ms (~435 m, corresponding to ~510 m after applying a 15% decompaction factor) between the central peak summit and annular trough (Fig. 5). However, the elevation markers show that this differential movement was not equally distributed over the central crater area, leading to the formation of terraces overlying high-angle faults (Fig. 3a, 4 and 5a) thereby forming a segmented central peak. Between terraces, the difference of elevation can reach hundreds of meters (Fig. 5a). The terraces and overall vertical motion are due to reactivation of concentric, syn-impact, high-angle and outward dipping fault of the central peak. The semi-brittle deformation of the overlying Hekkingen Formation is a manifestation of fault movement below LB. P-Cable data show extensional faulting of the Hekkingen Formation above the faults (Zoom 1 in Fig. 4). The bedding imbrications along post-impact faults (zoom 2 in Fig. 4) are interpreted as consequences of compressional stresses due to the flexure of the overburden. These key observations are compelling evidences of a post-Albian, upward displacement of the central peak with reactivation of sub-vertical, outward dipping faults.

To summarize, we have observed that the Mjølnir central peak was modified in at least two phases after impact: (1) A minor vertical uplift of ~10 meters occurred ~10 m.y. after open-marine shales draped a smooth central mound (Fig. 5b), documented by a seismic onlap of NW1 onto UB and (2) at least one post-Albian deformation phase triggered an uplift of the central peak of ~500 meters above the platform level. These vertical motions are seemingly linked to reactivations of several high-angle, impact-induced, concentric faults bounding the central peak.

5. Pre-impact stratigraphy

5.1 Seismic interpretation

The deeper structures of the impact crater are scrutinized on conventional reflection seismic data along line 3 (Fig. 6b). The Intra Snadd (IS) horizon is the most distorted and segmented horizon. The horizon is offset by normal faults and several listric faults in the outer domain of the crater. We observe numerous folds within [IS-LB] toward the inner part of the outer domain. Around the eastern central peak flank, at the transition between the outer domain to the annular basin, a major fault offsets the IS horizon deeper down, followed by increasing fault density. In the central domain, the IS horizon is over-steepening and rises towards the surface where we observe an abrupt truncation as IS toplaps LB. The previous observations can be extended to Top Kobbe (TK) and Top Klappmyss (TKL) with fault damage decreasing with horizon depth and gradually concentrating toward the crater center. However, the magnitude of stratigraphic uplift is less and less severe but affects a broader section of the seismic reflector as we go deeper in the stratigraphy. The number of outward-dipping, high-angle faults generally increases with depth and toward the crater center. The Top Havert (TH) horizon is mostly characterized by outward-dipping faults with increasing angle toward the central peak domain. The Top Permian (TP) horizon is distorted by a minor "bump" below the central peak, attributed to an imaging artifact (Tsikalas et al., 1998b).

5.2 Impact-disrupted zones

The deep conventional seismic data reveal new insights on fault geometry and deformation style in the impact-disrupted zone. The reflection seismic interpretation along line 3 (Fig. 6b) sheds light to brittle deformation style within the disturbance zone (DZ) beneath the central peak. The seismic Disturbance Zone (DZ) can be subdivided into three main regions (Fig. 6b):

(1) The allochthonous breccia zone, corresponding to the early post-impact crater infill and consisting in the violent surgeback of sediments in the transient crater shortly after impact (Unit II of the Ragnarok Formation; Dypvik et al., 2004).

(2) The autochthonous breccia zone showing intense folding and fracturing, with collapse of Jurassic-Triassic megablocks at the periphery of the central uplift region. The folds are likely resulting from the excavation/compression stage of the cratering process (Collins et al., 2012).

(3) The central peak zone has a conical shape with structural uplift as a dominant disruption at the Top Kobbe level and deeper. The magnitude of stratigraphic uplift is decreasing with depth. Despite the transparent seismic character below the crater center, we can confidently point-out that some of these outward-dipping faults are cross-cutting the whole impact-disrupted zone and could structurally couple the allochthonous brecciated rocks to the early Triassic sediments of the Havert Formation. The Upper Carboniferous – Lower Permian salt deposits were not disrupted by the impact (Fig. 6).

6. Discussion

Interpretation of high-resolution P-Cable seismic data at Mjølnir supports a detailed characterization of post-impact crater infill and vertical motions of the central peak (Fig. 7). We have distinguished six main post-impact stages at Mjølnir central peak. Despite a minor vertical movement shortly after Hekkingen shales deposition (Stage 1), the central peak remained idle while buried by at least ~700 meters of mud-rich, low-angle NW-SE prograding units in Barremian (Stage 2a) and NE-SW prograding units in Aptian-Albian (Stage 2b). The crater rims remained the most elevated topographic points of the buried crater up to stage 2b, at least ~40 m.y. after the Berriasian impact (Fig. 5b). The major post-impact deformation at Mjølnir central peak occurred post Albian (Stage 3) after a long period of inactivity. Following

platform uplift and erosion in the Cenozoic (Stage 4), the present-day summit of the central peak lies ~100 m below seabed and rises ~435 m above the rims.

6.1 A tectonized central peak at Mjølnir Crater?

Terrestrial and planetary complex craters with central peak elevated above the rim level are uncommon. To our knowledge, Mjølnir is the only example of such pristine crater morphology on Earth. One possible reason for this rare observation stems from the registry of terrestrial impact crater which is naturally biased towards exposed and/or eroded crater (Earth Impact Database).

To explain this particular feature at Mjølnir, Tsikalas and Faleide (2010) invoked differential compaction as a sole deformation mechanism. The argumentation relies on the hypothetical presence of denser rocks at the central peak based on a subtle, ~2 mGal, free-air gravity anomaly with a ~14 km radius centered at the central peak (Tsikalas et al., 1998c; Werner and Torsvik, 2010). However, density measurements at borehole 7329/03-U-01 (Fig. 5) show that the Jurassic and Triassic slabs of the central peak do not display increased density value after impact damage and stratigraphic uplift (Werner and Torsvik, 2010). Further gravity modelling demonstrates that the relative gravity high can be explained by a "normal" density contrast between post-impact Cretaceous sediments and the uplifted central peak rocks composed of shattered Triassic and Jurassic rocks (Fig. 7 in Werner and Torsvik, 2010). In addition, boreholes density measurements rather show that impact-shattered, uplifted rocks of central peaks tend to have increased porosity and lower density than their unaltered counterpart. A joint IOPD and ICS scientific drilling campaign, expedition 364, over the Cretaceous – Paleogene, 170 km-diameter Chicxulub Crater (Mexico) has reported increased porosity and lower density values in cores of shattered, uplifted rock samples of the peak ring area (Christeson et al., 2018). This is in contradiction with the main argument for differential compaction as causative mechanism for post-impact deformation at Mjølnir. Analogously to deeply buried salt bodies,

differential compaction is unlikely to reactivate vertical movement when a thick overburden covers a subtle vertical heterogeneity (Hudec and Johnson, 2007). Nevertheless, differential compaction may have tenuously modified the original shape of the central peak by ~10 meters after initial drape by marine shales (Stage 1 in Fig. 7). Differential compaction had a minor effect and cannot be solely invoked to explain the deformation of Mjølnir's central peak.

On planetary bodies, craters with elevated central peaks are generally called "central mound" craters. The most notorious example is the Gale Crater (Mars) and its 5 km-high central mound, Mt. Sharp. The formation of central mounds, and in particular of Mt. Sharp of Gale Crater, are subject of an on-going debate among Mars geologists. It is commonly accepted that Mt. Sharp formed as an erosional remnants of crater infill and/or as eolian deposits (Kite et al., 2013). Such processes are excluded for Mjølnir because the crater was buried and preserved from surficial processes shortly after impact.

An alternative mechanism by Kraft and Kristensen (2013) proposes a tectonic formation for Mt. Sharp. In fact, we argue below that tectonic stresses are the driving forces behind central peak deformation at the Mjølnir Crater.A tectonized crater is defined as "a crater that has been partially or completely modified by tectonic process after its formation" (Matias and Jurdy, 2014). This adjective is typically assigned to planetary impact craters by radar observation of rims, floor or ejecta layer. We propose to adapt this terminology to Mjølnir to term the structural deformation of its central peak by far-field tectonic stresses and resulting in a maximal elevation above the rim level. The arguments for a "tectonized central peak" at Mjølnir can be listed as follow:

(1) The top of Mjølnir's central peak is a rugged surface segmented by impact-induced, high-angle normal faults on the original crater floor (Fig 3b and 5). Bosumtwi is a 1.07 Ma, 10.5 km-diameter, complex impact crater with a pristine central peak that has an evident tectonic component on high-resolution seismic data (Scholtz et al., 2007). This

example suggests that large faults cross-cut the original central peak topography. Their existence is a pre-requisite for tectonic reactivation.

(2) We have identified post-impact reactivation of the impact-induced, high-angle faults at the central peak. Overlying those faults, the present-day central peak surface is parted in several concentric terraces with 100s of meters variation of elevation, suggesting post-impact normal fault displacements at the central peak (Figs. 3, 4 and 5).

(3) The overlying Hekkingen Formation shows a semi-brittle behavior with both plastic thinning and extensional faulting around the terraces (zoom 1 in Fig. 4). Compressional deformation is evidenced by bedding imbrications through thrust faulting of post-impact strata where the overburden starts flexuring (zoom 2 in Fig. 4). Similar compressional and extensional deformation regimes typically affect the flexured overburden over reactivated salt diapirs (Hudec and Jackson, 2012). The reactivation of deep faults and associated overburden flexure are compatible with a structural uplift triggered by far-field tectonic stresses.

(4) NW1 onlaps UB on the flanks of the central peak and illustrates a minor upward vertical movement (~10 m) at the central peak at time of NW1 deposition (Fig. 5). The deformation is coeval with a short-lived faulting event in the crater and surrounding platform.

(5) The Mjølnir Crater infill reconstruction at stage 2b (Albian) shows that the original ~35 m-high topography of the central peak (Fig. 3b) was passively buried by a km-thick overburden over 40 m.y. (Fig. 5). This absence of deformation at Mjølnir coincides with a period of tectonic quiescence in the SW Barents Sea (Stages 2a and 2b in Fig. 7).

(6) Reflection seismic shows that high-angle, outward-dipping faults can extend kilometers deep into the sedimentary platform and can mechanically couple the crater overburden with early Triassic shattered strata in the central crater area (Fig. 6). As a result,

contraction in deep impacted sedimentary layer could provoke displacement along deep-seated, high-angle faults of the central uplift zone (Fig. 5).

This set of evidences allows to ascribe the late modification of Mjølnir central peak to at least one phase of reactivation of impact-induced faults. Differential sediment loading could have played a minor role at the early stage of crater burial in Barremian (Stage 2a in Fig. 7).

6.2 A conceptual model for tectonized central peak formation

A conceptual model for the structural uplift of the central peak is summarized in Fig. 8. We propose that the structural uplift of the central peak is caused by a far-field compressional event at Paleogene times. The reactivation of the high-angle normal faults of the central peak in an upward motion and subsequent flexure of the overburden are consequences of that uplift.

Reflection seismic data indicate the presence of a typical "inverted-sombrero" shape Disturbance Zone (DZ) beneath the Mjølnir Crater (Fig. 6b; Tsikalas et al., 1998b). The DZ is thickest (~4 km thick) beneath the central peak. The seismic disturbance has a gradational lower boundary and contrasts sharply with the layer-cake sedimentary platform. There is a systematic loss of reflection coherency from the deeper and outer parts of the disturbance to its upper and central parts caused by a progression of seismic facies from disrupted layering and diffractions to chaotic and reflection-free zones (Tsikalas et al., 1998b). These seismic reflectivity patterns are interpreted as a volume of target rocks fractured and damaged by the bolide impact, as the intensity of brecciation and the amplitude of material displacement are expected to decrease from the center of the structure toward the periphery (Fig. 8).

This interpretation is consistent with the disintegration of the shallow target underneath the transient cavity into ~100 m large megablocks during the cratering process (Kenkmann et al., 2012). In addition, numerical modelling of impact on a terrestrial granitic target (Collins et al., 2004) demonstrates the shock wave imparted by the bolide impact severely damaged the target rocks.

Hence, after the impact, the weaker and less cohesive shattered target rocks of the DZ are prone to deformation. When the Bjarmeland Platform experienced episodes of crustal shortening, the DZ would then preferentially deform (Figs. 6 and 8), squeezed between stronger, un-impacted rocks. Because of the conservation of volume, the deformed rocks can only move upward resulting in the uplift of the Central Peak. The uplift of the peak naturally triggers reactivation of the pre-existing high-angle normal faults in an upward motion.

6.3 Regional implications

At the onset of the North Atlantic opening, the SW Barents Sea underwent several phases of tectonic activity from Late Jurassic to Early Cretaceous (Faleide et al., 1993; Gudlaugsson et al., 1998; Clark et al., 2013; Gac et al., 2018). Rifting events have been documented NW of the Bjarmeland Platform in the Fingerdjupet Subbasin and Hoop Fault Complex (Fig. 1; Collanega et al., 2017; Serck et al., 2017). Hence, the Berriasian-Valanginian tectonic event recorded in the interval [LB-UB] (Stage 1 in Fig. 7) in the outer crater domain (Fig. 3a) and surrounding platform is likely to be related to the same regional phase of rifting activity. The Mjølnir crater is located 100s of kilometers away from North Atlantic rifts and this large distance likely echoes on the short-lived, low intensity of the Early Cretaceous tectonic event on the Bjarmeland Platform. We assert that the first minor vertical motion of Mjølnir's central peak at Valanginian times is linked to a regional phase of activity linked with the onset of rifting in the North Atlantic.

A major phase of tectonic contraction affected the structural evolution of the Barents Sea in Late Cretaceous (Clark et al., 2013) or Paleogene (Stage 3 in Fig. 7; Mattingsdal et al., 2015). Halokinesis and anticline growth formed the Norvarg (Fig. 6a) and Samson domes (Mattos et al., 2016; Mattingsdal et al., 2015), two pillow structures located close to Mjølnir on the Bjarmeland Platform (Fig. 1). Although the timing of salt mobilization and post-impact central peak rise is unconstrained due to Neogene erosion, it is reasonable to believe that the

reactivation of Paleozoic salt layers and Mjølnir's central peak faults are correlated in the SW Barents Sea. Tectonic compression is the main triggering mechanism for salt-cored anticline growth over a thick overburden (Hudec and Jackson, 2012). Similarly, deep sub-vertical faults at Mjølnir are prone to reactivation and could easily accommodate the contraction and uplift of DZ. Net erosion in the crater area reaches ~2 km (Ktenas et al., 2017), meaning that the maximum paleo-depth of DZ was ~6 km prior to erosion (Ktenas et al., 2017). At such paleo-depth, Permian and Triassic sediments of the Bjarmeland Platform were competent enough to allow propagation of far-field tectonic stresses, mobilizing DZ brecciated rocks and salt layers in the SW Barents Sea (Fig. 1). We propose that Mjølnir's central peak structural rise responded to a regional contraction in Late Cretaceous - Paleogene.

One likely cause for compression is related to the transpression of the Greenland plate along the western margin of the Barents Sea as Greenland was moving northward after early Cenozoic break-up in the North-Atlantic. To assess the intraplate paleo-stress caused by transpression, Gac et al. (submitted) developed a numerical modelling approach combining a mechanical model of the Eurasia and Greenland lithosphere plates and plate kinematic models of the North-Atlantic. Two available, published plate kinematics models for the North-Atlantic were tested (Barnett-Moore et al., 2018; Gaina et al., 2009). Both models include transpression episodes at early Eocene. They both predict a strong Paleocene - early Eocene NNW-SSE compression component in the area of the Mjølnir crater during these transpression episodes.

Another possible mechanism causing compression in the Barents shelf is related to the Gravitational Potential Stress (GPStr) generated by elevated areas surrounding the Barents Shelf. Gac et al. (2016) estimated the GPSt within the North-Atlantic and Barents shelf from analysis of the residual geoid anomalies. Their estimate of the GPSt suggests that the Barents shelf is under compression since at least early Miocene.

7. Conclusion

A solid set of seismic evidences supports that Mjølnir post-impact modification is predominantly due to a structural rise of its central peak, presently ~435 meters above the rim level. We showed that, shortly after the Berriasian impact, the original Mjølnir Crater floor was a ~50 m depression on the seabed with one local high, a central mound rising ~35 m above the annular basin. The original crater topography was passively buried by fine-grained Barremian – Albian prograding units over 40 m.y. after impact. Differential compaction due to sediment loading over the annular basin may have tenuously enhanced the central peak by ~10 m after draping by marine shales. Lying beneath a thick overburden, deep, impact-induced faults were reactivated by uplift of segments of the central peak, causing semi-brittle deformation of the overlying Hekkingen Formation. We propose that impact-shattered rocks beneath the central peak were mobilized and uplifted in response to one or more contractional events in Late Cretaceous - Paleogene in the SW Barents Sea causing the reactivation of impact-induced faults. This study demonstrates that central peaks have a strong structural component, stemming from the structural uplift and/or collapse stage of the impact-cratering process. We propose that central peaks are prone to vertical deformation by far-field tectonic stresses and that the tectonic context should always be carefully considered when investigating proven and potential impact structures.

Acknowledgements

The authors wish to thank VBPR, TGS and Spectrum for allowing to publish their multiclient data. VBPR colleagues are acknowledged for stimulating discussions and comments. J.I Faleide and S. Planke acknowledge support from the Research Council of Norway through its Centers of Excellence funding scheme, Project Number 223272 (CEED) and 228107 (ARCEx). Peter

Klitzke and an anonymous reviewer are acknowledged for constructive comments that helped to improve significantly the quality of the initial manuscript.

References

Barnett-Moore, N., D.R. Müller, S. Williams, J. Skogseid, and M. Seton (2018), A reconstruction of the North Atlantic since the earliest Jurassic, Basin Res., 126, doi:10.1111/bre.12214.

Bellwald, B., Planke, S., Piasecka, E.D., Matar, M.A., Andreassen, K., 2018. Ice-stream dynamics of the SW Barents Sea revealed by high-resolution 3D seismic imaging of glacial deposits in the Hoop area. Marine Geology v402, p. 165-183. https://doi.org/10.1016/j.margeo.2018.03.002

Bellwald, B., Planke, S., Lebedeva-Ivanova, N., Piasecka, E.D., Andreassen, K., 2019. High-resolution assemblage along a buried glacio-erosive surface in the SW Barents Sea by P-Cable 3D seismic data. Geomorphology v332, p.33-50. https://doi.org/10.1016/j.geomorph.2019.01.019

Christeson, G.L. et al., 2018. Extraordinary rocks from the peak ring of the Chixculub impact crater: P-wave velocity, density, and porosity measurements from IODP/ICDP Expedition 364. Earth Planet. Sci. Lett., 495, p.1-11 https://doi.org/10.1016/j.epsl.2018.05.013

Clark, S. A., Glorstad-Clark, E., Faleide, J. I., Schmid, D., Hartz, E. H., & Fjeldskaar, W., 2013. Southwest Barents Sea rift basin evolution: comparing results from backstripping and time-forward modelling. Basin Research v26(4), p. 550–566. doi:10.1111/bre.12039

Collanega, L., Massironi, M., Breda, A., Kjølhamar, B.E., 2017. Onset of N-Atlantic rifting in the Hoop Fault Complex (SW Barents Sea): An orthorhombic dominated faulting? Tectonophysics v706-707, p. 59-70. https://doi.org/10.1016/j.tecto.2017.04.003

Collins, G.S., Melosh, H.J., & Osinski, G.R., 2012. The Impact-Cratering Process. Elements, v8(1), p. 25–30. doi:10.2113/gselements.8.1.25

Collins, G.S., Melosh, H.J., Ivanov, B.A., 2004. Modelling damage and deformation in impact simulations. Meteorit Planet Sci v39, p 217-231. https://doi.org/10.1111/j.1945-5100.2004.tb00337.x

Corseri, R., Faleide, T.S., Faleide, J.I., Midtkandal, I., Serck, C.S., Trulsvik, M., Planke, S., 2018. A diverted submarine channel of Early Cretaceous revealed by high-resolution seismic data, SW Barents Sea. Marine and Petroleum Geology v98, p. 462-476. https://doi.org/10.1016/j.marpetgeo.2018.08.037

Dypvik H., Attrep M. Jr., 1999. Geochemical signals of the late Jurassic, marine Mjølnir impact. Meteorit Planet Sci v34, p. 393–406. DOI 10.1111/j.1945-5100.1999.tb01348.x

Dypvik, H., Mørk. A., Smelror, M., Sandbakken, P.T., Tsikalas, F., Vigran, J.O., Bremer, G.M.A., Nagy, J., Gabrielsen, R.H., Faleide, J.I., Bahiru, M., Weiss, H., 2004. Impact breccia and ejecta from Mjølnir crater in the Barents Sea – The Ragnarok Formation and Sindre Bed. Nor Geologisk Tidsskrift v84, p.143–167. ISSN 029-196X.

Dypvik, H., Tsikalas, F., Smelror, M., 2010. The Mjølnir impact event and its consequences. Springer. Berlin-Heidelberg. DOI: 10.1007/978-3-540-88260-2

Earth Impact Database. Planetary and Space Science Centre. University of New Brunswick, Canada. http://www.passc.net/EarthImpactDatabase/New%20website_05-2018/Index.html)

Faleide, J.I., Vågnes, E., Gudlaugsson, S.T., 1993. Late Mesozoic-Cenozoic evolution of the south-western Barents Sea in a regional rift-shear tectonic setting. Marine and Petroleum Geology v10, p.186-214. https://doi.org/10.1016/0264-8172(93)90104-Z

Faleide, J.I., Bjørlykke, K., Gabrielsen, R.H., 2010. Geology of the Norwegian Continental Shelf. In Petroleum Geoscience (ed K Bjørlykke), pp. 467–499. Springer, Berlin. https://doi.org/10.1007/978-3-642-02332-3_22

Faleide, T.S., Midtkandal, I., Planke, S., Corseri, R., Faleide, J.I., Serck, C.S., Nystuen, J.P., 2019. Characterisation and development of Early Cretaceous shelf platform deposition

and faulting in the Hoop area, southwestern Barents Sea—constrained by high-resolution seismic data. Norwegian Journal of Geology 99, 1-20. https://dx.doi.org/10.17850/njg99-3-7

Gac, S., Hansford, P.A., Faleide, J.I., 2018, Basin modelling of the SW Barents Sea. Marine and Petroleum Geology v95, p. 167-187. https://doi.org/10.1016/j.marpetgeo.2018.04.022

Gac, S., Klitzke, P., Minakov, A., Faleide, J.I., Scheck-Wenderoth, M., 2016, Lithosphere strength and elastic thickness of the Barents Sea and Kara Sea, Tectonophysics, v691, p.120-132. https://doi.org/10.1016/j.tecto.2016.04.028

Gaina, C., L. Gernigon, and P. Ball (2009), Palaeocene Recent plate boundaries in the NE Atlantic and the formation of the Jan Mayen microcontinent, J. Geol. Soc., 166, 601-616, doi:10.1144/0016-76492008-112.

Glimsdal, S., Pedersen, G.K., Langtangen, H.P., Shuvalov V., Dypvik, H., 2007. Tsunami generation and propagation from the Mjølnir asteroid impact. Meteorit Planet Sci v42, p. 1473–1493. https://doi.org/10.1111/j.1945-5100.2007.tb00586.x

Golombek, M., et al. (2012), Selection of the Mars Science Laboratory Landing Site, Space Sci Rev, 170(1-4), 641-737. doi: 10.1007/s11214-012-9916-y

Grieve, R.A.F., Personen, L.J., 1992. The record of terrestrial impact cratering. Tectonophysics v216, p.1-30.

Grundvåg, S.-A., Marin, D., Kairanov, B., Śliwińska, K.K., Nøhr-Hansen, H., Escalona, A., Olaussen, S., 2017. The Lower Cretaceous succession of the northwestern Barents Shelf: Onshore and offshore correlations. Marine and Petroleum Geology v86, p. 834-857. DOI: 10.1016/j.marpetgeo.2017.06.036.

Gudlaugsson, S.T., 1993. Large impact crater in the Barents Sea. Geology v21, p. 291–294. doi: 10.1130/0091-7613(1993)021<0291:LICITB>2.3.CO;2

Gudlaugsson, S.T., Faleide, J.I., Johansen, S.E., Breivik, A.J., 1998. Late Palaeozoic structural development of the south-western Barents Sea. Marine and Petroleum Geology v15, p.73-102. http://dx.doi.org/10.1016/S0264-8172(97)00048-2.

Hudec, M.R., Jackson, M.P.A., 2007. *Terra Infirma*: Understanding salt tectonics. Earth-Science Reviews v82, p. 1-28. https://doi.org/10.1016/j.earscirev.2007.01.001

Hudec, M.R., Jackson, M.P.A., 2012. *De Re Salica:* Fundamental principles of salt tectonics. In: Roberts, D.G., Bally, A.W. (Eds) Regional geology and tectonics: Phanerozoic passive margins, cratonic basins and global tectonic maps. Elsevier. https://doi.org/10.1016/C2010-0-67672-3

Kenkmann, T., Collins, G.S., Wünnemann, K., 2012. The modification stage of crater formation. In: Impact cratering: Processes and Products, Eds: Osinski, G.R., Pierazzo, E. Blackwell Publishing. p. 60-75. Kenkmann, T., Collins, G. S., & Wünnemann, K. (2012). The Modification Stage of Crater Formation. Impact Cratering, 60–75. doi:10.1002/9781118447307.ch5

Kenkmann, T., Poelchau, M.H., Wulf, G., 2014. Structural geology of impact craters. Juornal of Structural Geology v62, p. 156-182. http://dx.doi.org/10.1016/j.jsg.2014.01.015

Kite, E.S., Lewis, K.W., Lamb, M.P., Newman, C.E., Richardson, M.I., 2013. Geology v41 (5), p. 543-546. https://doi.org/10.1130/G33909.1

Kraft, M.D., Christensen, P.R., 2013. Tectonic formation of Mount Sharp, Gale Crater, Mars. 44th Lunar and planetar Science Conference. https://www.lpi.usra.edu/meetings/lpsc2013/pdf/3106.pdf

Ktenas, D., Henriksen, E., Meisingset, I., Nielsen, J.K., Andreassen, K., 2017. Quantification of the magnitude of net erosion in the southwest Barents Sea using sonic velocities and compaction trends in shales and sandstones, Marine and Petroleum Geology v88, p. 826-844. doi:10.1016/j.marpetgeo.2017.09.019.

Lebedeva-Ivanova, N., Polteau, S., Bellwald, B., Planke, S., Berndt, C., Stokke, H.H., 2018. Toward one-meter resolution in 3D seismic. Leading Edge v37, p. 818–828. https://doi.org/10.1190/tle37110818.1

Matias, A., Jurdy D.M., 2014. Deformed Crater (Tectonized). In: Encyclopedia of Planetary Landforms. Springer, New York, NY. https://doi.org/10.1007/978-1-4614-9213-9

Mattos, N.H., Alves, T.M., Omosanya, K.O., 2016. Crestal fault geometries reveal late halokinesis and collapse of the Samson Dome, Northern Norway: Implications for petroleum systems in the Barents Sea. Tectonophysics v690. p. 76-96. http://dx.doi.org/10.1016/j.tecto.2016.04.043

Mattingsdal, R., Høy, T., Simonstad, E., Brekke, H., 2015. An updated map of structural elements in the southern Barents Sea. 31st Geological Winter Meeting. Poster Session. http://www.npd.no/Global/Norsk/2-Tema/Geologi/Strukturelementer/Poster-Nye_strukturelementer_BHS%C3%98.pdf

Midtkandal, I., Faleide, J.I., Faleide, T.S., Serck, C.S., Planke, S., Corseri, R., Dimitriou, M., Nystuen, J.P., 2019a. Lower Cretaceous Barents Sea strata: epicontinental basin configuration, timing, correlation, and depositional dynamics. Geological Magazine, 1-19. DOI:10.1017/S0016756819000918 1.

Midtkandal, I., Faleide, T.S., Faleide, J.I., Planke, S., Anell, I., Nystuen, J.P., 2019b. Nested intrashelf platform clinoforms—Evidence of shelf platform growth exemplified by Lower Cretaceous strata in the Barents Sea. *Basin Res*. p. 1–8. https://doi.org/10.1111/bre.12377

Planke, S., and Berndt, C., 2004. Apparatus for seismic measurements. UK Pat. No. GB 2401684.

Poag, C.W., Koeber, C., Reimold, W.U., 2004. The Chesapeake Bay Crater: Geology and Geophysics of Late Eocene Submarine Impact structure. Springer. Berlin-Heidelberg, p. 3. https://doi.org/10.1007/978-3-642-18900-5

Poelchau, M.H., Kenkmann, T., Kring, D.A., 2009. Rim uplift and crater shape in Meteor Crater: Effects of target heterogeneities and trajectory obliquity. J. Geophys. Res., 114, E01006, https://doi.org/10.1029/2008JE003235

Scholtz, C.A., Karp, T., Lyons, R.P., 2007. Structure and morphology of the Bosumtwi impact structure from seismic reflection data. Meteorit Planet Sci v42, p. 549-560. https://doi.org/10.1111/j.1945-5100.2007.tb01060.x

Serck, C.S., Faleide, J.I., Braathen, A., and Kjølhamar, B., 2017. Jurassic to Early Cretaceous basin configurations(s) in the Fingerdjupet Subbasin, SW Barents Sea. Marine and Petroleum Geology v86, p. 874-891. http://dx.doi.org/10.1016/j.marpetgeo.2017.06.044

Shuvalov, V., Dypvik, H., Tsikalas, F., 2002. Numerical simulations of the Mjølnir marine impact crater. J Geophys Res v107 doi 10.1029/2001JE001698

Sættem, J., Poole, D.A.R., Ellingsen, L., Sejrup, H.P., 1992. Glacial geology of outer Bjørnøyrenna, southwestern Barents Sea. Marine Geology 103, p. 15-51. https://doi.org/10.1016/0025-3227(92)90007-5

Tsikalas, F., Gudlaugsson, S.T., Faleide, J.I., 1998a. Collapse, infilling, and postimpact deformation at the Mjølnir impact structure, Barents Sea. Geol Soc Am Bull v110, p. 537–552. https://doi.org/10.1130/0016-7606(1998)110<0537:CIAPDA>2.3.CO;2

Tsikalas, F., Gudlaugsson, S.T., Faleide, J.I., 1998b. The anatomy of a buried complex impact structure: The Mjølnir Structure, Barents Sea. J Geophys Res v103, p. 30469–30484. 0148-0227/98/97JB-03389509.00

Tsikalas, F., Gudlaugsson, S.T., Eldholm, O., Faleide, J.I., 1998c. Integrated geophysical analysis supporting the impact origin of the Mjølnir Structure, Barents Sea. Tectonophysics v289, p. 257–280. https://doi.org/10.1016/S0040-1951(97)00234-5

Tsikalas, F., Faleide, J.I., 2007. Postimpact structural crater modification due to sediment loading: An overlooked process. Meteorit Planet Sci v42, p. 2013–2029. https://doi.org/10.1111/j.1945-5100.2007.tb00557.x

Tsikalas, F., Faleide, J.I., 2010. Postimpact deformation due to sediment loading: The Mjølnir Paradigm. In: Dypvik, H., Tsikalas, F., Smelror, M. (Eds), The Mjølnir impact event and its consequences. Spring. Berlin-Heidelberg. DOI: 10.1007/978-3-540-88260-2

Werner, S.C., Torsvik, T.H., 2010. Downsizing the Mjølnir impact structure, Barents Sea, Norway. Tectonophysics v483, p. 191-202. doi:10.1016/j.tecto.2009.08.036

Fig. 1 Location map of the Mjølnir impact crater, with structural elements and salt structures in the SW Barents Sea. The structural elements are taken from Faleide et al. (2010).

Fig. 2 Seismic-chronostratigraphic chart of the Bjarmeland Platform. The yellow star indicates the time when the bolide impacted the Hekkingen Formation, ~142 Ma ago, forming the Mjølnir impact crater. The Ragnarok Formation (hatched pattern) is composed of impact breccia and is subdivided into unit I and unit II (Dypvik et al., 2004). The seismic data type displayed on the chart is 2D high-resolution P-Cable seismic. SF: Seafloor; URU: Upper Regional Unconformity; NE: North East prograding unit; NW: North West prograding unit; UB: Upper Boundary; TD: Top Disturbance; LB: Lower Boundary. P-Cable seismic data courtesy of TGS and VBPR.

Fig. 3 (A) Uninterpreted (top) and interpreted (bottom) 2D P-Cable seismic section along line 1. The color-code for the post-impact interval is indicated in the seismic-chronostratigraphic chart (Fig. 2) (B) P-Cable seismic section along line 1 flattened on the UB horizon. The original crater relief is represented by the yellow horizon TD. The yellow dots are key morphometric reference points along the original crater surface TD. The black solid lines represent internal reflectors within the [TD-UB] unit. The dotted lines represent the inferred continuation of the internal reflections across the URU truncation. The white zone represents the eroded section of [TD-UB]. P-Cable seismic data courtesy of TGS and VBPR.

Fig. 4 Uninterpreted (top) and interpreted (bottom) 2D P-Cable seismic section along line 2. The yellow dots are key morphometric reference points along the original crater surface TD. Two detailed zoom examples on Line 2 (bottom) show evidence of different stress regimes in the overburden. P-Cable seismic data courtesy of TGS and VBPR.

Fig. 5 (A) Interpreted P-Cable seismic section (line 1) centered on the central peak. Faults are depicted by thin black lines (B) Interpreted P-Cable seismic section flattened along

seismic horizon NE3b and focused on the annular basin and central peak domains (Fig. 2), NE3b horizon is represented by a thick horizontal black line. The color code is displayed in Fig. 2. The yellow dots are key morphometric reference points along the original crater surface TD. The black solid lines represent internal reflectors within each sequence. The dotted lines represent the inferred continuation of the reflections across the URU truncation. Note that the quaternary interval has been removed from the reconstruction to ease the visualization of continuous reflection patterns across the truncation. The two vertical grey bands overlain distortions induced by seismic flattening near two shallow faults. P-Cable seismic data courtesy of TGS and VBPR.

Fig. 6 Interpreted 2D seismic reflection data A) across the Norvarg salt dome and B) the Mjølnir structure (line 3). The color code divides the disturbance zone DZ due to impact in three brecciated areas. IS: Intra Snadd, TK: Top Kobbe, TKL: Top Klappmyss, TH: Top Havert, TP: Top Permian. Seismic data courtesy of TGS and Spectrum.

Fig. 7 Summary chart depicting the main seismic events at the Mjølnir central peak from impact to quaternary (left column). We have divided the post-impact burial history of the central peal in four key stages. (Right column) Tectonic calendar of the Bjarmeland Platform from earliest Cretaceous to Paleogene. The arrow symbols indicate the nature of the tectonic event: extension (thick black line), compression (blue arrows) and regional uplift (red arrows). HALIP: High Arctic Large Igneous Province.

Fig. 8 Conceptual model of formation of the Mjølnir tectonized central peak where tectonic compression mobilizes impact-shattered rocks and reactivates impact-induced faults segmenting the central peak domain. A) Central peak before tectonic compression in Albian. The crater relief is covered by a km-thick flat-layered and prograding sediments (Fig. 5b) while the impact disturbance zone (DZ) shows a typical “inverted-sombrero” shape. The typical “inverted-sombrero” shape of DZ at Mjølnir Crater is reproduced

from Dypvik et al. (2004) with a paleo-depth scale that accounts for the post-impact sediment thickness in Albian. B) Central peak at the end of tectonic compression in Paleogene. The impact disturbance zone DZ, composed of shattered rocks, is squeezed at depth by far-field compression. The mobilization of brecciated rocks below the central peak reactivates impact-induced faults, uplifting the central peak and provoking the flexure of the thick post-impact overburden analogue to salt doming and diapiric rise. The present-day erosion is marked by a discontinuous black line. The approximate paleo-depth scale accounts for 2 km of net erosion in the crater area (Ktenas et al., 2017). The color code of the post-impact strata is shown in Fig. 2. Note the discontinuity in the vertical scale to illustrate the effect of compression in both post- and pre-impact strata. TP: Top Permian.

Fig.1

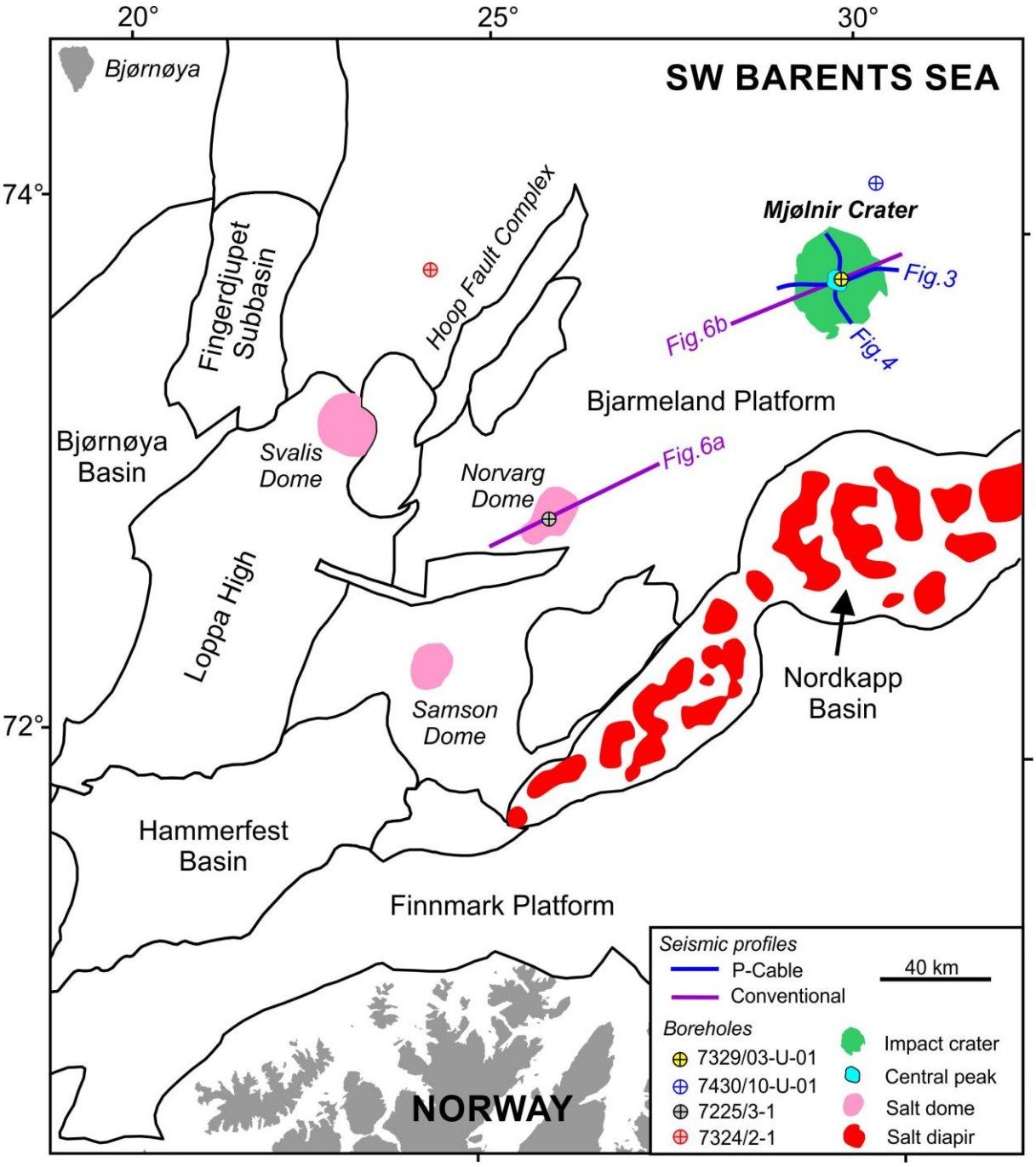
20°
25°
30°
74°
72°
SW BARENTS SEA
Bjørnøya
Fingerdjupet Subbasin
Hoop Fault Complex
Mjølnir Crater
Fig.3
Fig.6b
Fig.4
Bjarmeland Platform
Bjørnøya Basin
Svalis Dome
Norvarg Dome
Fig.6a
Loppa High
Samson Dome
Nordkapp Basin
Hammerfest Basin
Finnmark Platform
NORWAY
Seismic profiles
P-Cable
Conventional
40 km
Boreholes
7329/03-U-01
7430/10-U-01
7225/3-1
7324/2-1
Impact crater
Central peak
Salt dome
Salt diapir

Fig. 2

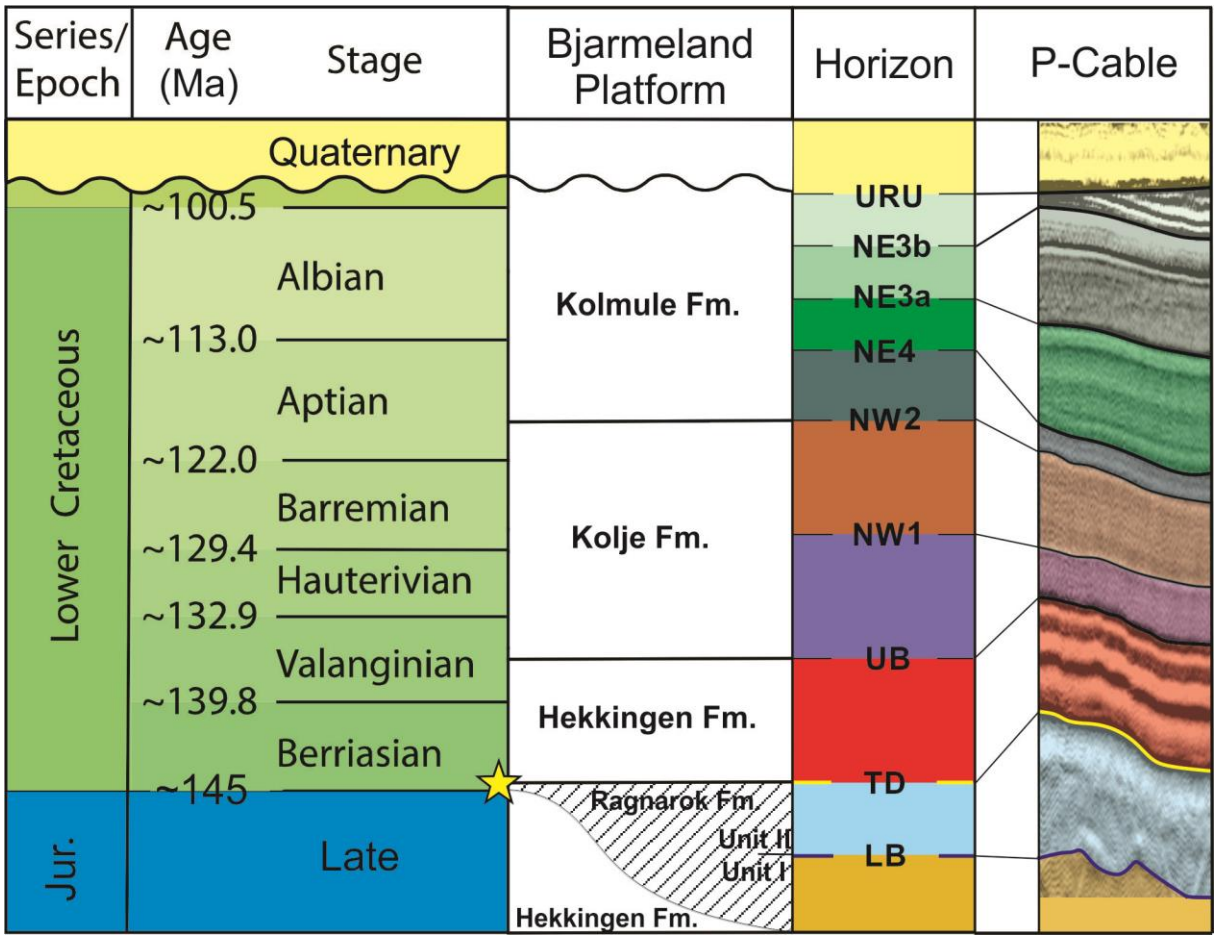
Series/ Epoch
Age (Ma)
Stage
Bjarmeland Platform
Horizon
P-Cable
Quaternary
~100.5
Albian
~113.0
Aptian
~122.0
Barremian
~129.4
Hauterivian
~132.9
Valanginian
~139.8
Berriasian
~145
Late
Lower Cretaceous
Jur.
Kolmule Fm.
Kolje Fm.
Hekkingen Fm.
Ragnarok Fm.
Unit II
Unit I
Hekkingen Fm.
URU
NE3b
NE3a
NE4
NW2
NW1
UB
TD
LB

Fig. 3

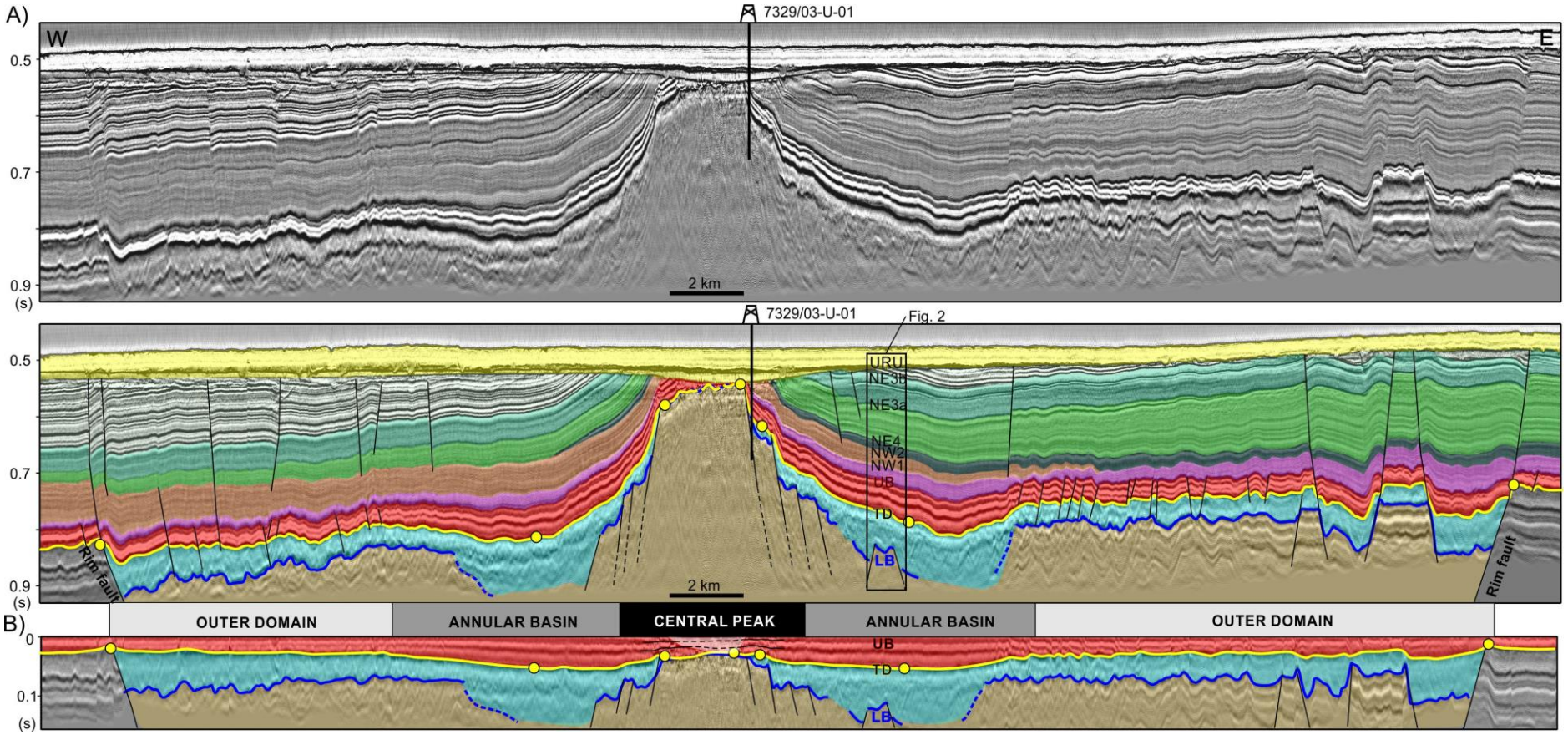
A)
W
E
7329/03-U-01
0.5
0.7
0.9
(s)
2 km
7329/03-U-01
Fig. 2
URU
NE3b
NE3a
NE4
NW2
NW1
UB
TD
LB
Rim fault
Rim fault
2 km
B)
OUTER DOMAIN
ANNULAR BASIN
CENTRAL PEAK
ANNULAR BASIN
OUTER DOMAIN
0
0.1
(s)
UB
TD
LB

Fig. 4

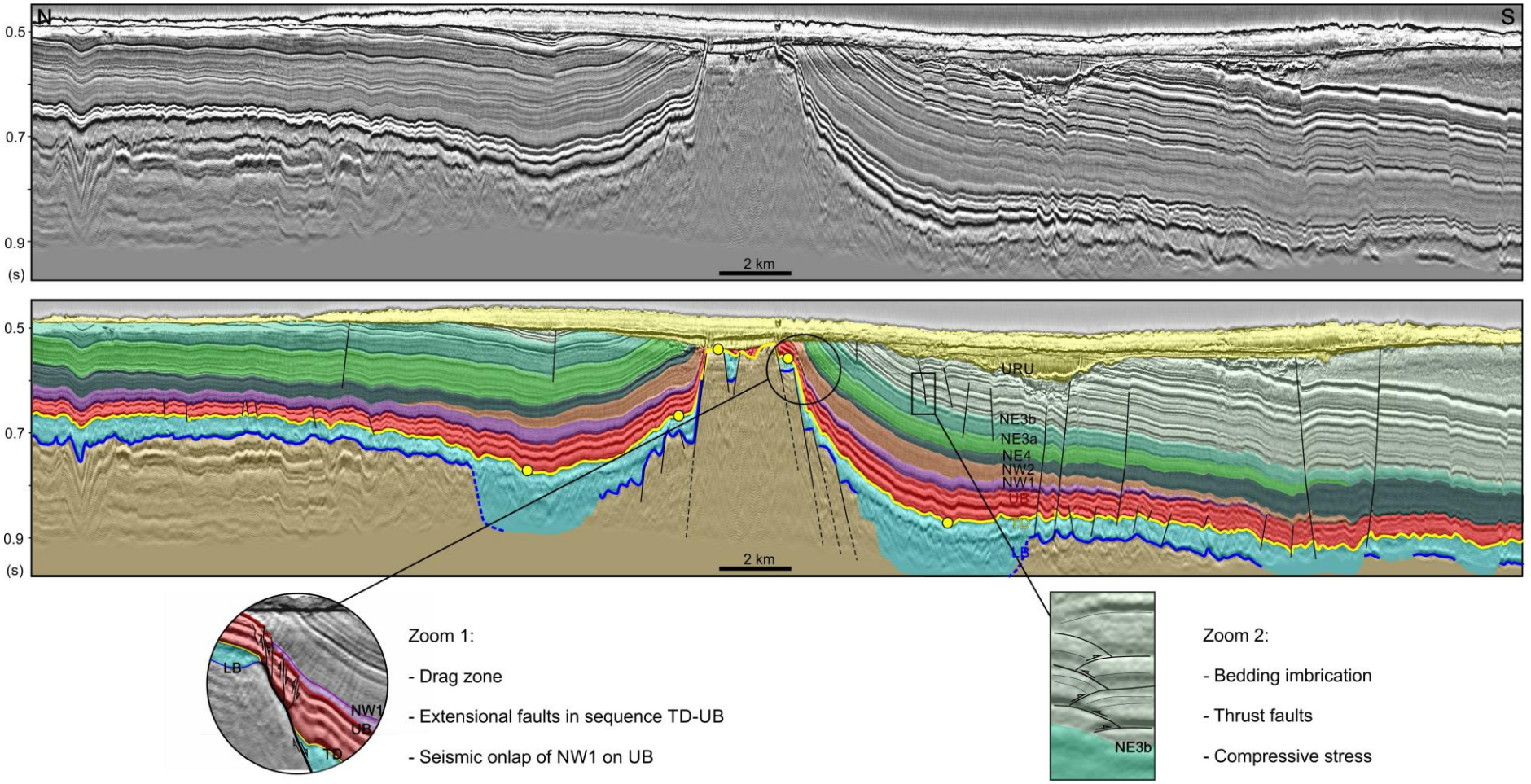
N
S
0.5
0.7
0.9
(s)
2 km
URU
NE3b
NE3a
NE4
NW2
NW1
UB
TD
LB
Zoom 1:
- Drag zone
- Extensional faults in sequence TD-UB
- Seismic onlap of NW1 on UB
Zoom 2:
- Bedding imbrication
- Thrust faults
- Compressive stress

Fig. 5

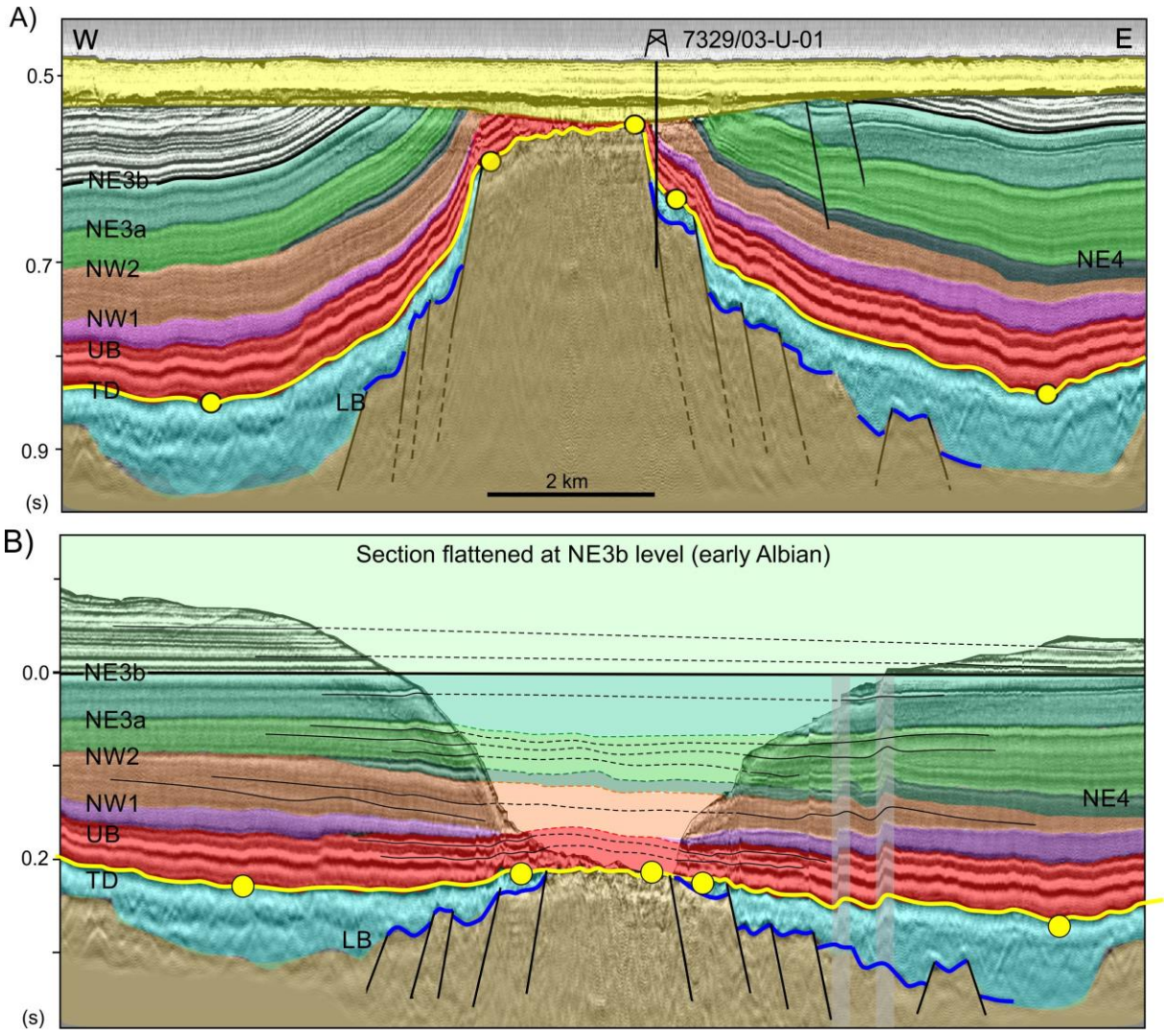
A)
W
7329/03-U-01
E
0.5
NE3b
NE3a
NW2
0.7
NW1
UB
TD
LB
NE4
0.9
(s)
2 km
B)
Section flattened at NE3b level (early Albian)
0.0
NE3b
NE3a
NW2
NW1
UB
0.2
TD
LB
NE4
(s)

Fig. 6

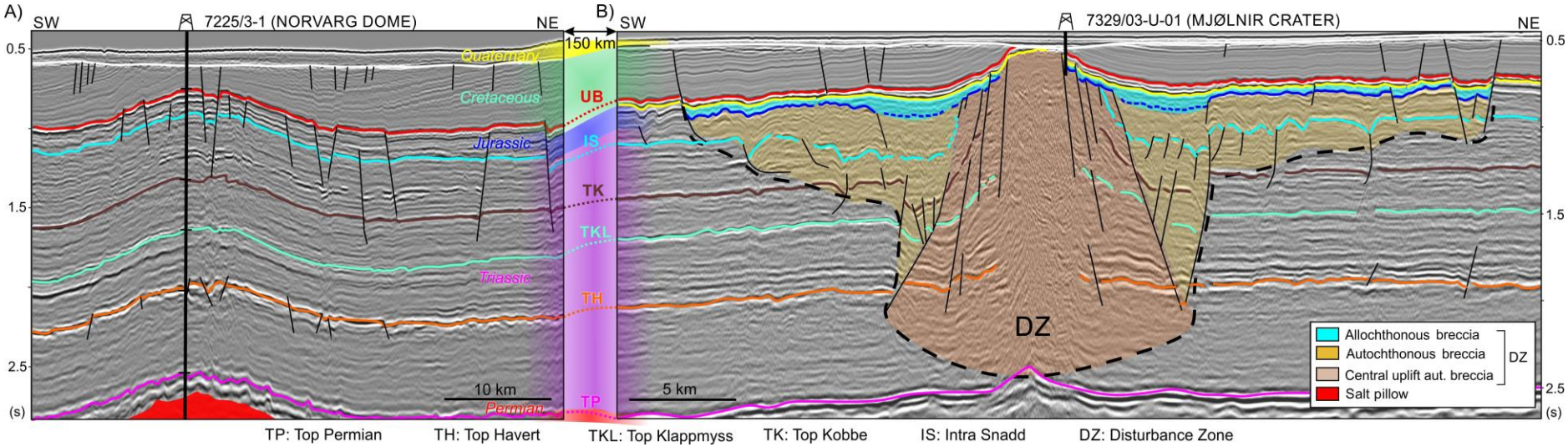
A)
SW
7225/3-1 (NORVARG DOME)
NE
B)
SW
7329/03-U-01 (MJØLNIR CRATER)
NE
150 km
0.5
1.5
2.5
(s)
Quaternary
Cretaceous
Jurassic
Triassic
Permian
UB
IS
TK
TKL
TH
TP
10 km
5 km
DZ
Allochthonous breccia
Autochthonous breccia
Central uplift aut. breccia
Salt pillow
DZ
TP: Top Permian
TH: Top Havert
TKL: Top Klappmyss
TK: Top Kobbe
IS: Intra Snadd
DZ: Disturbance Zone

Fig. 7

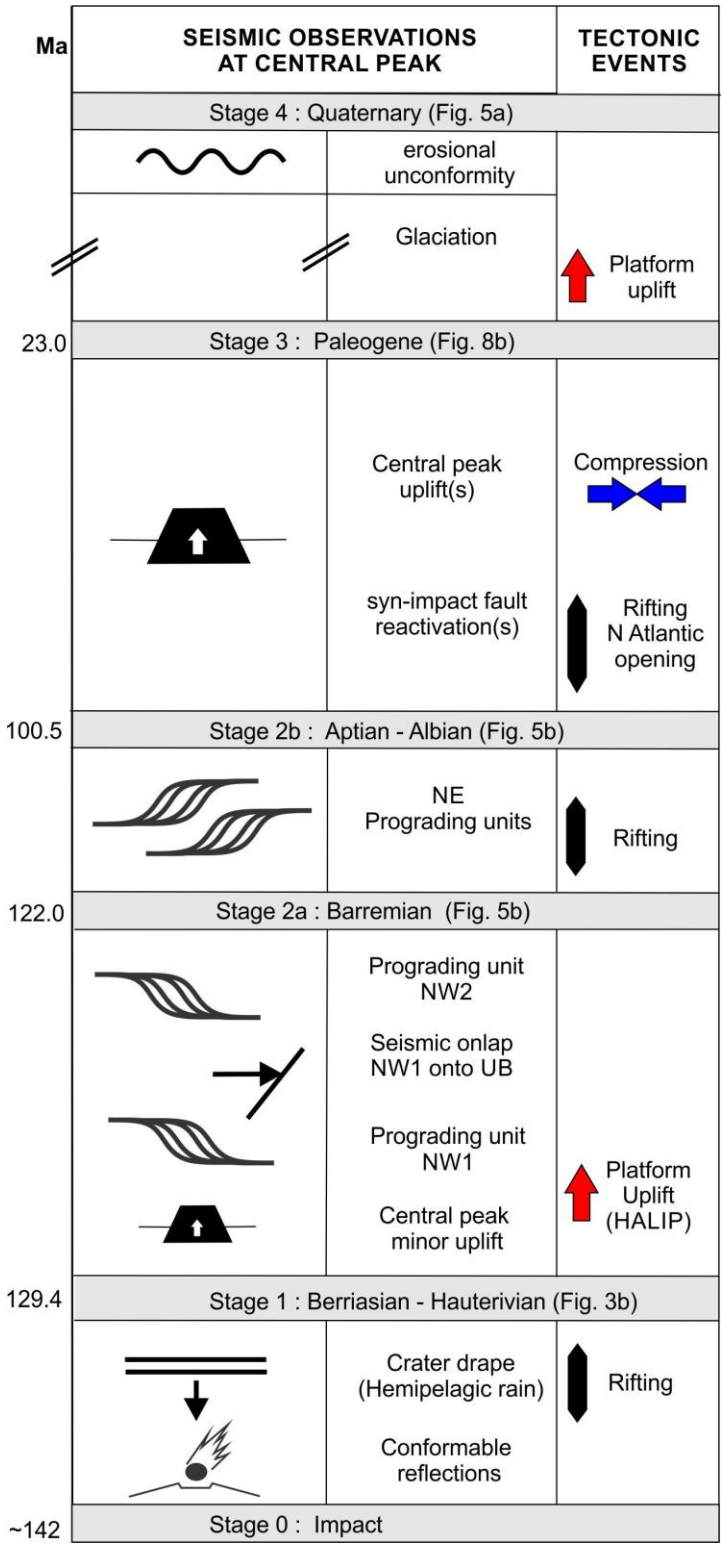
Ma
SEISMIC OBSERVATIONS AT CENTRAL PEAK
TECTONIC EVENTS
Stage 4 : Quaternary (Fig. 5a)
erosional unconformity
Glaciation
Platform uplift
23.0
Stage 3 : Paleogene (Fig. 8b)
Central peak uplift(s)
Compression
syn-impact fault reactivation(s)
Rifting N Atlantic opening
100.5
Stage 2b : Aptian - Albian (Fig. 5b)
NE Prograding units
Rifting
122.0
Stage 2a : Barremian (Fig. 5b)
Prograding unit NW2
Seismic onlap NW1 onto UB
Prograding unit NW1
Central peak minor uplift
Platform Uplift (HALIP)
129.4
Stage 1 : Berriasian - Hauterivian (Fig. 3b)
Crater drape (Hemipelagic rain)
Conformable reflections
Rifting
~142
Stage 0 : Impact

Fig. 8

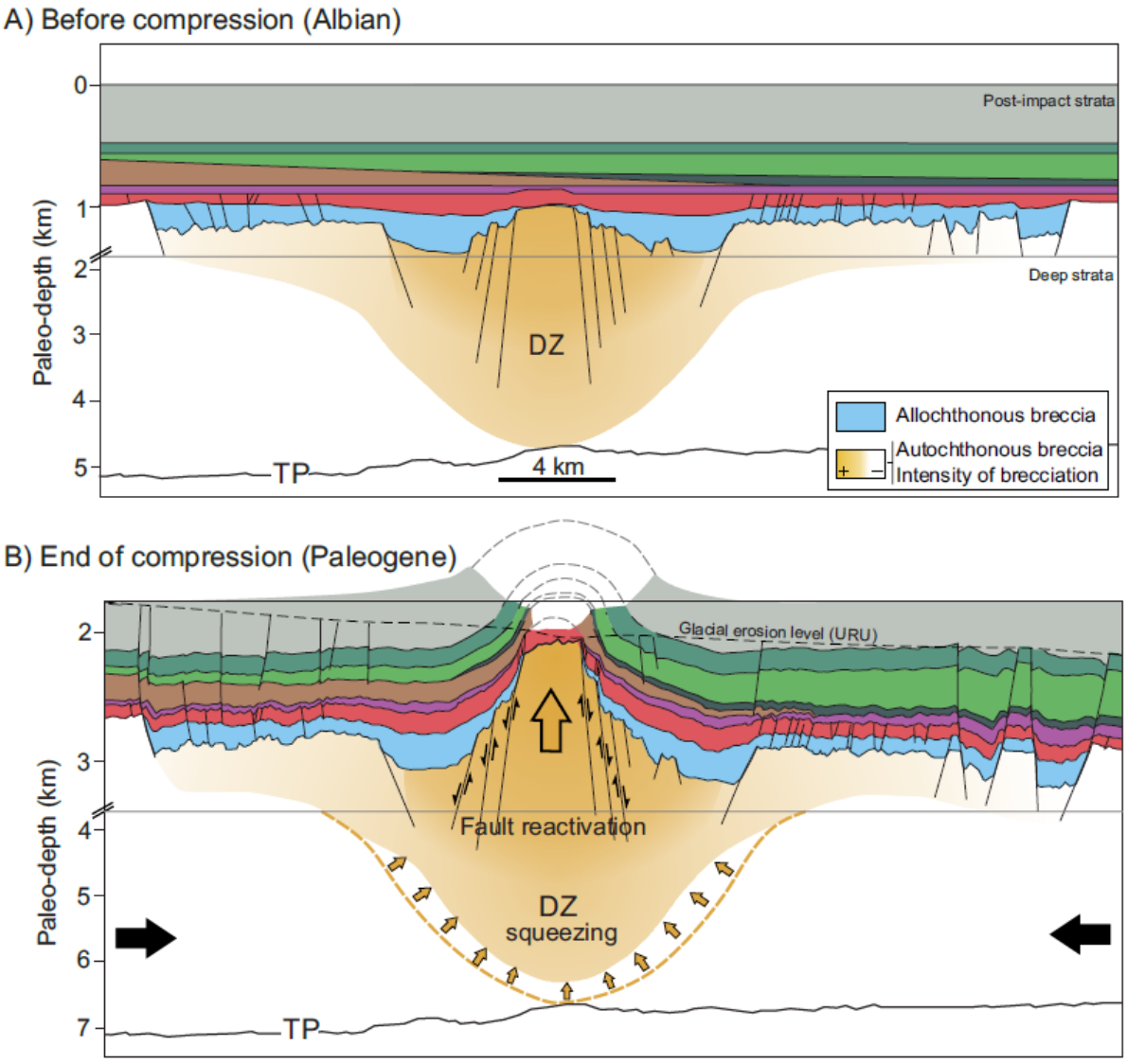
A) Before compression (Albian)
Paleo-depth (km)
0
1
2
3
4
5
Post-impact strata
Deep strata
DZ
TP
4 km
Allochthonous breccia
Autochthonous breccia
Intensity of brecciation
+
–
B) End of compression (Paleogene)
Paleo-depth (km)
2
3
4
5
6
7
Glacial erosion level (URU)
Fault reactivation
DZ
squeezing
TP